NANO LETTERS

Letter

pubs.acs.org/NanoLett

Terahertz Spectroscopy of Individual Single-Walled Carbon Nanotubes as a Probe of Luttinger Liquid Physics

Joel D. Chudow,[†] Daniel F. Santavicca,[†,‡] and Daniel E. Prober*[,†]

[†]Department of Applied Physics, Yale University, New Haven, Connecticut 06511, United States

[‡]Department of Physics, University of North Florida, Jacksonville, Florida 32224, United States

ABSTRACT: Luttinger liquid theory predicts that collective electron excitations due to strong electron−electron interactions in a one-dimensional (1D) system will result in a modification of the collective charge-propagation velocity. By utilizing a circuit model for an individual metallic single-walled carbon nanotube as a nanotransmission line, it has been shown that the frequency-dependent terahertz impedance of a carbon nanotube can probe this expected 1D Luttinger liquid behavior. We excite terahertz standing-wave resonances on individual antenna-coupled metallic single-walled carbon nanotubes. The terahertz signal is rectified using the nanotube contact nonlinearity, allowing for a low-frequency readout of the coupled terahertz current. The charge velocity on the nanotube is determined from the terahertz spectral response. Our measurements show that a carbon nanotube can behave as a Luttinger liquid system with charge-propagation velocities that are faster than the Fermi velocity. Understanding what determines the charge velocity in low-dimensional conductors is important for the development of next generation nanodevices.

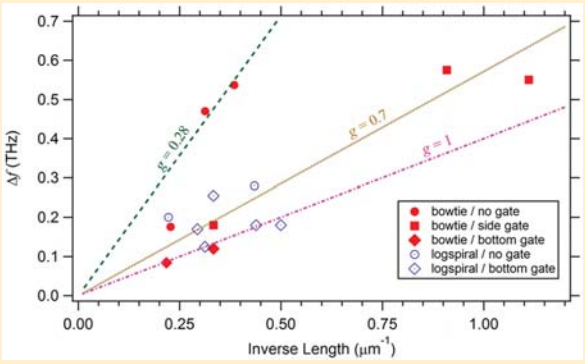

KEYWORDS: *Carbon nanotubes, Luttinger liquid, terahertz spectroscopy, one-dimensional conductors*

Carbon nanotubes are a prototypical experimental system for the verification of fundamental one-dimensional (1D) electron-conduction models and serve as attractive candidates for diverse potential applications. Due to their small diameter, the electron wave function is quantized around the circumference of a nanotube, resulting in an effectively 1D electronic system.[1−4] Landau's Fermi liquid theory breaks down in 1D due to weak screening of the Coulomb interaction. Instead, such a strongly interacting 1D electron gas forms a correlated state known as a Luttinger liquid, in which the low-energy electron excitations are collective bosonic soundlike density waves of spin and charge.[5−7] A unitless order parameter g, known as the Luttinger parameter, quantifies the strength and nature of electron−electron interactions, with $g < 1$ for repulsive interactions and $g = 1$ for a noninteracting system such as a Fermi liquid.

A hallmark of the Luttinger liquid model is a power-law dependence of tunneling conductivity on temperature and bias voltage. Theoretical work has predicted $g \approx 0.28$ for metallic carbon nanotubes.[8] Several reports on tunneling into ropes and individual carbon nanotubes claim agreement with this prediction.[1,9−12] However, other possible explanations, such as dynamical Coulomb blockade, could result in the same observed behavior.[13−15] Furthermore, experiments on multi-walled carbon nanotubes yielded similar results over an unexpectedly wide range of conditions.[7,16,17] These results leave unresolved the question of whether Luttinger liquid behavior can be observed in the electrical-transport properties of carbon nanotubes.

Another signature of the correlated behavior of electrons in 1D is the phenomenon of spin-charge separation. A 1D system supports collective excitations of charge and spin bosonic modes, which are separable and propagate at different velocities. The charge mode is commonly known as a plasmon, and the spin modes are referred to as neutral modes because they do not convey any net charge. The manifestation of spin-charge separation via tunneling conduction has been experimentally observed for parallel nanowires in a GaAs−AlGaAs heterostructure[18] and also in measurements of an electrostatically gated 1D system.[19]

The propagation characteristics of the charge-carrying plasmon excitations in 1D systems are dependent on the strength of the electron−electron interactions. In the present work, we utilize the frequency-dependent absorption of an individual metallic single-walled carbon nanotube to access this faster charge-mode velocity. The high-frequency properties of a single-walled carbon nanotube[20] can be understood by treating the nanotube and ground plane as a transmission line. This model, first proposed by Bockrath[21] and developed in detail by Burke,[22] yields the transmission-line properties, including phase

Received: April 10, 2016
Revised: June 28, 2016
Accepted: July 14, 2016

ACS Publications © XXXX American Chemical Society

DOI: 10.1021/acs.nanolett.6b01485
Nano Lett. XXXX, XXX, XXX−XXX

velocity v_p and characteristic impedance Z_{char}. This model is consistent with Luttinger liquid theory for describing the interacting electrons in a 1D system.

The nanotube is modeled with the effective circuit given in Figure 1. Following Burke,[22] included in this model is a kinetic inductance, L_K, accounting for the kinetic energy stored in the motion of the charge carriers, and a quantum capacitance, C_Q, accounting for the finite band energy needed to add charge to the nanotube, as well as an electrostatic capacitance, C_{ES}, which is typical for a wire and a ground plane but also has a contribution due to electron−electron interactions. Carbon nanotubes possess two conduction channels from the orbital degeneracy of the two Dirac points in the unit sub-lattice, and each channel allows for spin degeneracy with electrons as either spin-up or spin-down.[22] Thus, the complete model is composed of four connected transmission lines in parallel that interact with one another through their common connection to C_{ES}. L_K is $\frac{h}{2e^2 v_F} \approx 16$ nH/μm per channel, corresponding to ≈4 nH/μm for the four parallel channels.[22] L_K exceeds the magnetic inductance $L_M \approx$ pH/μm by several orders of magnitude, and so L_M is omitted in the model. Due to the low density of states, the quantum capacitance is comparable in magnitude to the electrostatic capacitance C_{ES}, and both must be considered. C_{ES} between the nanotube and the environment, including the ground plane, is ∼50 aF/μm. C_Q of each of the four channels is given by $\frac{2e^2}{hv_F} \approx 100$ aF/μm. This value was experimentally confirmed by Ilani et al.[3]

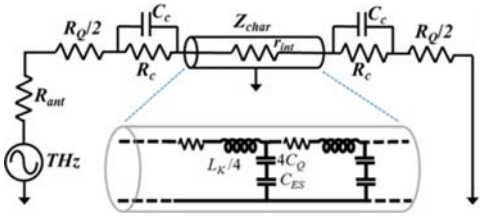

Figure 1. Equivalent circuit model of a carbon nanotube in a planar antenna geometry acting as THz source with impedance R_{ant}. The enlargement highlights the effective transmission-line circuit diagram for the nanotube composed of an infinite series of resistances, inductances, and capacitances per unit length.

AC voltage excitations result in the dynamical charging−discharging of the nanotube, and it can be shown[22] that these can accommodate four collective modes, one of which conveys charge, the plasmon or charge mode, and three that do not transfer any net charge, the spin or charge-neutral modes. The charge mode corresponds to currents through all the spin-up and -down channels in the same direction, and neutral modes are spin-up currents in one direction and spin-down currents in the other. This represents the separation of spin and charge as is expected in an interacting Luttinger liquid system. Because the neutral modes do not convey any charge, they do not interact through C_{ES} and will not couple to electric fields.

We also include a term to account for damping due to electron scattering within the nanotube, denoted as an internal distributed resistance per unit length, r_{int}. This r_{int} for the best experimentally measured nanotubes is found to be ∼1 kΩ/μm at low temperature,[25,26] which we assume for our simulations. In the circuit diagram, we incorporate the intrinsic quantum of resistance split equally between each end of the nanotube. The quantum of resistance of h/e^2 = 25.8 kΩ for each quantum channel becomes $R_Q = h/4e^2$ = 6.45 kΩ for the four parallel channels of the nanotube.[2,3] In addition to the quantum of resistance R_Q, an additional contact resistance R_c between the nanotube and electrodes is included in parallel with a contact coupling capacitance C_c between the 3D metal electrodes and the nanotube. The contact resistance R_c arises from the

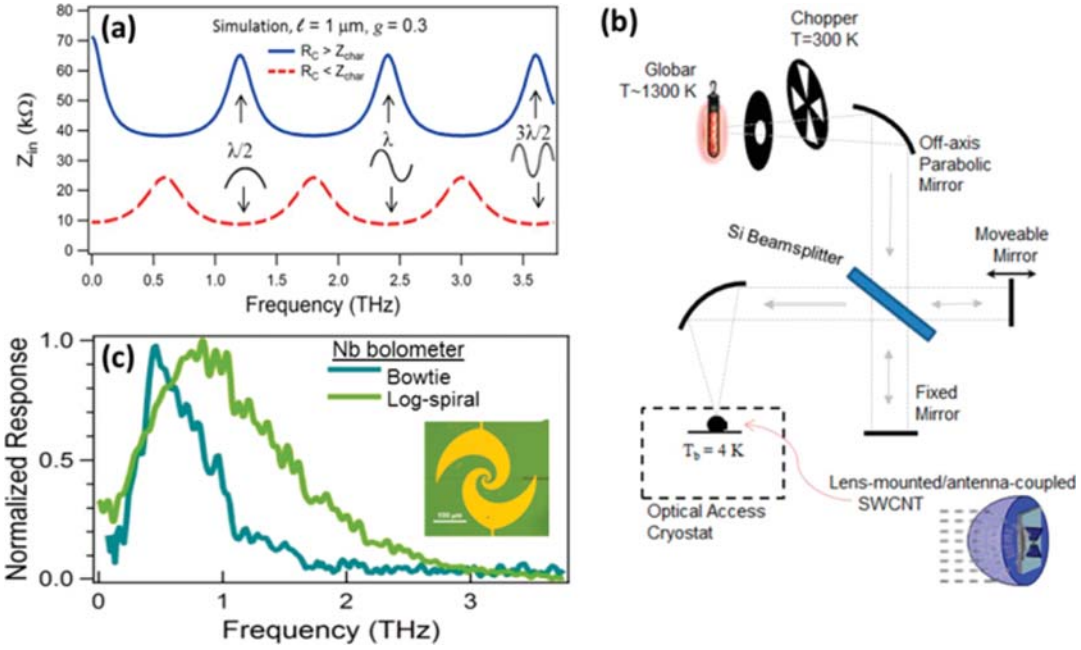

Figure 2. (a) Predicted standing-wave resonances on a carbon nanotube in two limits of R_t compared to Z_{char}, with r_{int} = 1 kΩ/μm. (b) Schematic of Fourier transform interferometer and antenna-coupled nanotube device for broadband THz generation and spectral response measurement. (c) Spectral response of niobium superconducting microbridge bolometers, with bowtie and log-spiral antenna structures showing the background system spectral response.

DOI: 10.1021/acs.nanolett.6b01485
Nano Lett. XXXX, XXX, XXX−XXX

imperfect transparency of the metal−nanotube interface; R_c is zero for a perfect contact. Even though the associated contact capacitance C_c is in fact a distributed capacitance between the electrode and the length of the nanotube, it is modeled as a parallel-lumped element here for simplicity.

Calculating the wave velocity of the neutral modes, which do not include C_{ES}, gives $v_{neutral} = 1/\sqrt{L_k C_Q}$, equal to the Fermi velocity, $v_F = 8 \times 10^5$ m/s. If repulsive electron−electron interactions are now accounted for with the inclusion of C_{ES}, the wave velocity for the four parallel channels is found to be greater than v_F,

$$v_{plasmon} \approx \sqrt{\frac{1}{\frac{L_K}{4}C_{tot}}} \approx \sqrt{\frac{4}{L_K C_{ES}} + \frac{1}{L_K C_Q}} \quad (1)$$

where $C_{tot}^{-1} = (4C_Q)^{-1} + C_{ES}^{-1}$. The ratio of these two velocities is the dimensionless Luttinger parameter g, which quantifies the strength of the electron−electron interaction. The Luttinger parameter can also be determined via a capacitive relation composed of C_Q and C_{ES} expressing the reduction of the electron−electron interactions by the screening of the electrostatic Coulomb force:

$$g \equiv \frac{v_F}{v_{plasmon}} = \sqrt{\frac{C_{tot}}{4C_Q}} = \sqrt{\frac{C_{ES}}{4C_Q + C_{ES}}} \quad (2)$$

For a very weakly interacting system, $C_{ES} \gg C_Q$, $C_{tot} \to C_Q$, and $g = 1$. For a strongly interacting system, $C_{ES} \ll C_Q$, $C_{tot} \to C_{ES}$, and $g \to 0$. The characteristic impedance, $Z_{char} = \sqrt{\frac{L_K}{C_{tot}}} = \sqrt{\frac{L_K}{4C_Q} + \frac{L_K}{C_{ES}}} = \frac{1}{g}\frac{h}{8e^2}$, also varies with g. For the four parallel quantum channels in an individual nanotube, $g = 0.3$ corresponds to $Z_{char} \approx 10$ kΩ.

The wave velocity can be determined by examining the power coupling to a finite-length mismatched transmission line, which acts as a quarter-wave impedance transformer.[23] Plasmon standing-wave resonances occur when the nanotube length l corresponds to integral multiples of half-wavelengths. This situation occurs when $l = n\frac{\lambda}{2} = n\frac{v_p}{2f}$, where n is a positive integer, which gives resonant frequencies $f_n = n\frac{v_F}{2lg}$ with frequency spacing $\Delta f = \frac{v_F}{2lg}$ directly related to v_p and g. For $R_t < Z_{char}$, where $R_t = R_c + R_Q/2$ is the total terminating contact resistance, input impedance minima occur at integer multiples of a half-wavelength, and input impedance maxima occur at odd multiples of a quarter-wavelength. For $R_t > Z_{char}$, the reverse is true, such that the input impedance maxima occur at half-wavelengths, and input impedance minima occur at odd multiples of a quarter-wavelength, as shown in Figure 2a. For the actual nanotube devices studied, R_t has a large range of values (20−500 kΩ) but is always in the $R_t > Z_{char}$ regime.

We previously reported measurements of rf and THz detection in individual carbon nanotubes, distinguishing between two response mechanisms: bolometric detection due to heating the nanotube electrons with a temperature-dependent resistance and the rectified THz response due to nonthermal electrical-contact nonlinearities.[27−29] The nonthermal detection mechanism is dominant at low bias current. The nonlinear detection mechanism rectifies the THz current passing through the nanotube contacts. This rectification gives a DC response. Variation in the nanotube's input impedance will modify the power coupling into the nanotube and, hence, the THz current that flows through the contacts. With this mechanism, we obtain an interferogram of each antenna-coupled nanotube device in our Fourier transform interferometer setup. (The few samples that exhibited measurable bolometric detection had poor signal-to-noise ratios and did not produce meaningful interferograms.) The gate voltage, bias current, and temperature have a significant impact on the signal-to-noise ratio of the measurement.[29] We employ considerable averaging, a low scan rate, long scan times, and zero padding of the interferograms[30] by a factor of 2 to produce a clear spectral response. The spectral response is analyzed by attempting to identify the minima of power coupling or current flow, characterized by a dip in the spectral response (e.g., see Figure 3). Each dip in the THz response corresponds to a maximum in the input impedance. The frequency location of such a feature or the spacing of repetitive dips yields the value of Δf that is used to determine the charge propagation velocity v_p and, hence, g.

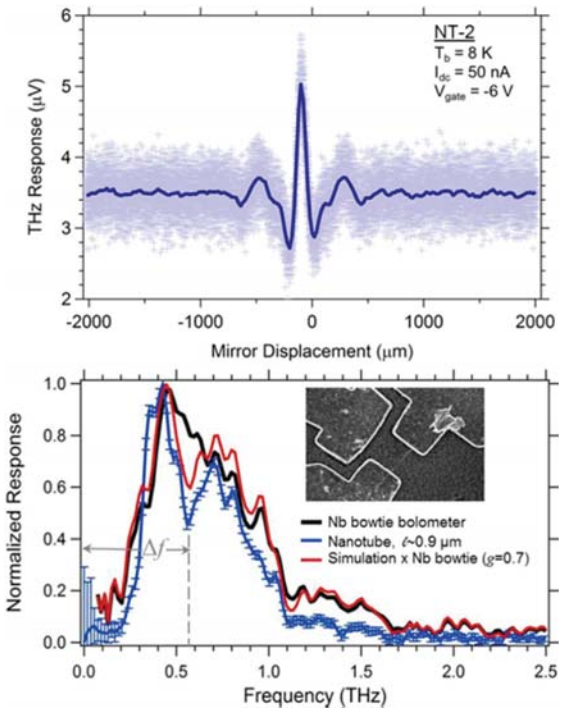

Figure 3. (Top) Measured individual and averaged interferograms of 0.9 μm long carbon-nanotube device in bowtie antenna with side-gate using the nanotube contact nonlinearity as the THz detection mechanism. (Bottom) Normalized spectral response from Fourier transform of nanotube interferogram compared to a niobium bowtie background. There is a dip in the nanotube THz response at ≈0.6 THz, revealing the frequency spacing Δf. A simulation of the nanotube response from the transmission-line model, normalized by the system bandwidth determined by measuring a Nb microbolometer, reproduces this feature with a value of $g = 0.7$.

The equivalent circuit model used to represent the antenna as a voltage source can also influence the expected resonance behavior within the nanotube. The THz signal incident on the nanotube has an impedance approximately equal to that of the antenna (≈100 Ω), which is much less than the nanotube resistance (>10 kΩ), so it approximates a voltage source. Treating the antenna as an asymmetric or antisymmetric voltage source, and the relative distribution of the contact resistance on each end of the nanotube will affect the input

DOI: 10.1021/acs.nanolett.6b01485
Nano Lett. XXXX, XXX, XXX−XXX

impedance of the nanotube and, thus, the magnitude of THz coupling into the nanotube. However, the resonant-frequency locations generally remain unmodified. For the special case of an antisymmetric voltage source with contact resistance divided evenly between the two ends of the nanotube, the even n resonances do not appear due to destructive interference on the nanotube transmission line. These resonances can reemerge as the difference between the contact resistances on each end of the nanotube increases. Also, with increasing values of C_c, the magnitude of each resonant feature increases as a function of frequency. In our model, we treat the antenna as an asymmetric voltage source and assume that the contact resistance is evenly divided between the two ends of the nanotube, each shunted by a small parallel C_c, as shown in Figure 1.

Measurements of the dynamical conductance up to 10 GHz of single-walled carbon nanotubes with lengths over 100 μm did not observe any clear resonant behavior.[24] This result was attributed to the damping of the plasmons by a large internal resistance, >100 kΩ, which dissipates the plasmon in a long nanotube and prevents the formation of standing-wave resonances. The scattering length due to electron−phonon interactions in a high-quality metallic single-walled carbon nanotube can be as a large as 10 μm at low temperature, and these nanotubes exhibit internal resistances per unit length of ∼1 kΩ/μm.[25,26] Thus, short nanotubes, on the order of a few microns, measured at low temperatures are necessary to observe the predicted standing-wave resonance behavior. These shorter lengths necessitate higher measurement frequencies, ∼THz. Zhong and collaborators[31] sought to measure v_p using THz time-domain reflectometry of very-brief-duration electrical pulses in μm-long individual nanotube devices. They found resonances corresponding to propagation at the Fermi velocity. A faster plasmon velocity was not observed. Ngai and Kim[32] theoretically considered this experiment and concluded that this experimental approach will excite all four modes available in a nanotube (three neutral spin modes and one charge mode), so the response may be dominated by the slower spin modes. They, like Burke, propose an alternate measurement scheme of v_p based on coupling the charge plasmon mode to an applied oscillating electric field and observing AC conductance peaks versus drive frequency for μm-long metallic carbon nanotubes. Other theoretical treatments of the interaction of high-frequency radiation with carbon nanotubes to extract v_p have been reported.[22,33−35] THz detection and generation utilizing bundles of carbon nanotubes have also been reported.[36,37] Plasmon resonances are predicted to be revealed in the THz thermal-emission spectrum of bundles of nanotubes, but no evidence of the resonances was observed.[38] The use of heterogeneous bundles of nanotubes instead of a single individual nanotube may complicate and possibly prevent the observation of this behavior.

To efficiently deliver THz radiation to an individual single-walled metallic carbon nanotube, we utilize a quasi-optical coupling technique employing a lens and planar antenna geometry.[39] The broadband THz generation and spectral response measurement is achieved using a Fourier transform interferometer (FTIR) with the nanotube mounted in an optical-access cryostat that is cooled with liquid helium,[40] as shown in Figure 2b. The THz source is a silicon carbide globar (thermal source) heated to approximately 1300 K. The source is on−off modulated with a room-temperature chopping wheel, permitting an AC measurement of the low-frequency response to the THz power using a lock-in amplifier. Low-pass filters on the cryostat window eliminate signals at frequencies above the THz range. The system is maintained in a dry environment during measurement to minimize THz absorption by water vapor. For a nanotube in the FTIR system, features corresponding to standing-wave resonances appear in addition to the system spectral response. These periodic features (specifically, dips in the absorbed power) deviate from the antenna and optical-system spectral background and correspond to standing-wave resonances along the finite-length nanotube.

The DC properties and the THz response as a function of bias current at low temperature for a ≈0.9 μm long nanotube in a bowtie antenna (sample NT-2) were previously reported.[29] Using a bias current of 100 nA (low bias-current region) for nonlinear detection and a gate voltage of V_{gate} = −6 V, we measure an interferogram at low temperature (T ≈ 4 K), as shown in Figure 3. The gate voltage biases the quasi-metallic nanotube in the metallic state. The particular values of the bias current and gate voltage were chosen to optimize the signal-to-noise ratio of the rectified THz response. In addition to the average result of ≈100 scans, we also plot the individual data points during each scan to show the variation. Figure 3 also shows the normalized spectral response achieved from a Fourier transform of the interferogram average, as well as the standard error for each frequency data point from the collection of scans. Several other interferograms of this sample were taken at differing bias currents and gate voltages and exhibited the same behavior. There is a prominent dip in the spectral response at f ≈ 0.6 THz in comparison to the background response of the bowtie antenna and optical system. This background response is determined by measuring the bolometric response of a superconducting niobium (Nb) microbolometer with the same antenna geometry.[40] The microbolometer has frequency-independent absorption over the measurement bandwidth and does not exhibit length-dependent spectral-response variations. Assuming the nanotube has high-resistance contacts ($R_t > Z_{char}$), the dip at ≈0.6 THz corresponds to a half-wavelength resonance. At this resonance, there is an increased input impedance, which decreases the coupling of THz current to the nanotube and hence decreases the THz current through the nanotube contacts. The contacts partially rectify the THz current. The frequency of this dip is reproducible for the several measurements at different biasing conditions. Using this measured value of Δf ≈ 0.6 THz as the first resonance yields g ≈ 0.7, corresponding to $v_p \approx 1.1 \times 10^6$ m/s. Higher-order resonances, which would be expected to occur at 1.2 THz (full wavelength) and 1.8 THz (three-halves wavelength), are beyond the bandwidth of the bowtie antenna and FTIR system. Simulations carried out using AWR Microwave Office of this nanotube as a transmission line with its measured length and total resistance, assuming r_{int} = 1 kΩ/μm,[25] are used to determine the effective total capacitance per unit length, C_{tot}, that will produce an impedance maximum at f ≈ 0.6 THz. In Figure 3, we plot the product of this simulation and the normalized spectral response of the antenna system as measured with the Nb bolometer. We find good agreement between the measured nanotube THz response data and simulation with a value of C_{tot} ≈ 200 aF/μm, which is consistent with g ≈ 0.7. An uncertainly of ±0.05 THz in the experimental value of Δf would correspond to an uncertainty of ±11 aF/μm in C_{tot} and an uncertainly of ±0.06 in g.

Using this nonlinear THz-detection approach, we have measured other individual antenna-coupled metallic single-

DOI: 10.1021/acs.nanolett.6b01485
Nano Lett. XXXX, XXX, XXX−XXX

Table 1. Summary of Properties for Devices Discussed[a]

	contact structure		biasing conditions					
sample length (μm)	antenna	gate	I_{bias} (nA)	V_{gate} (V)	R (kΩ)	Δf (THz)	g	C_{tot} (aF/μm)
0.9	bowtie	side-gate	50	−6	40	0.55	0.74	240
1.1	bowtie	side-gate	30	−3	50	0.6	0.65	150
3.2	log-spiral	bottom-gate	5	−32	700	0.18	0.70	200
4.6	bowtie	bottom-gate	20	−0.6	31	0.09	0.97	350
3.1	log-spiral	bottom-gate	10	−32	600	0.13	0.99	390
3.2	bowtie	no gate	100		32	0.46	0.27	30
2.6	bowtie	no gate	3		900	0.54	0.29	35

[a]The measured DC resistance R includes the contact resistances, quantum resistance, and internal nanotube resistance. Also included is the value of C_{tot} determined from fitting simulations to the measured data.

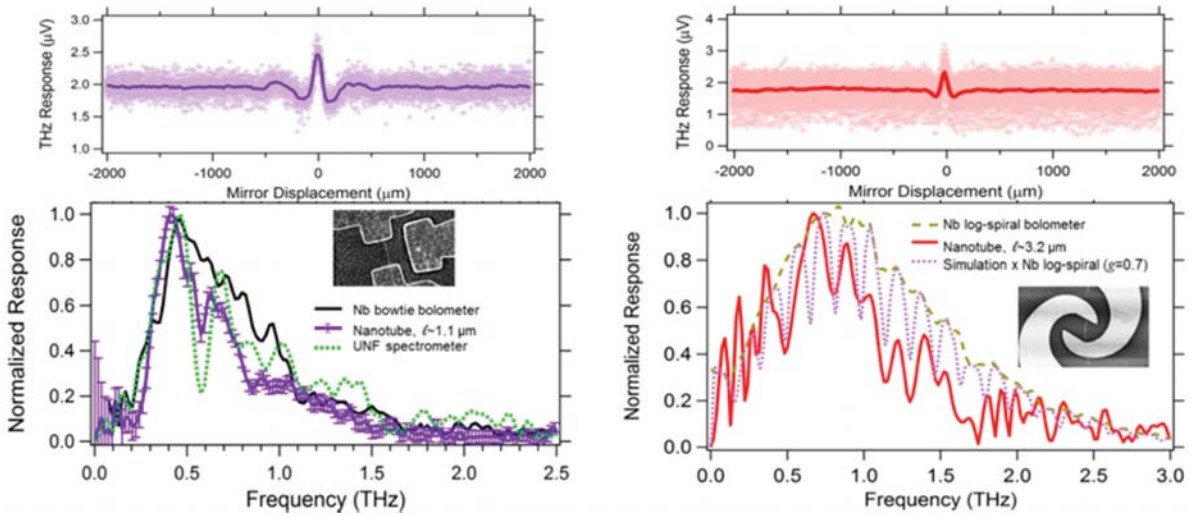

Figure 4. (Left) Interferogram and normalized spectral response of a 1.1 μm long nanotube device in a bowtie antenna with a side-gate compared to the system background. Also shown are the data from the same sample measured in a different FTIR system showing the same dip in the THz response at ~0.55 THz. (Right) Results for a 3.2 μm long nanotube device in log-spiral antenna with bottom-gate showing periodic features compared to a Nb log-spiral background and a simulation corresponding to g = 0.7.

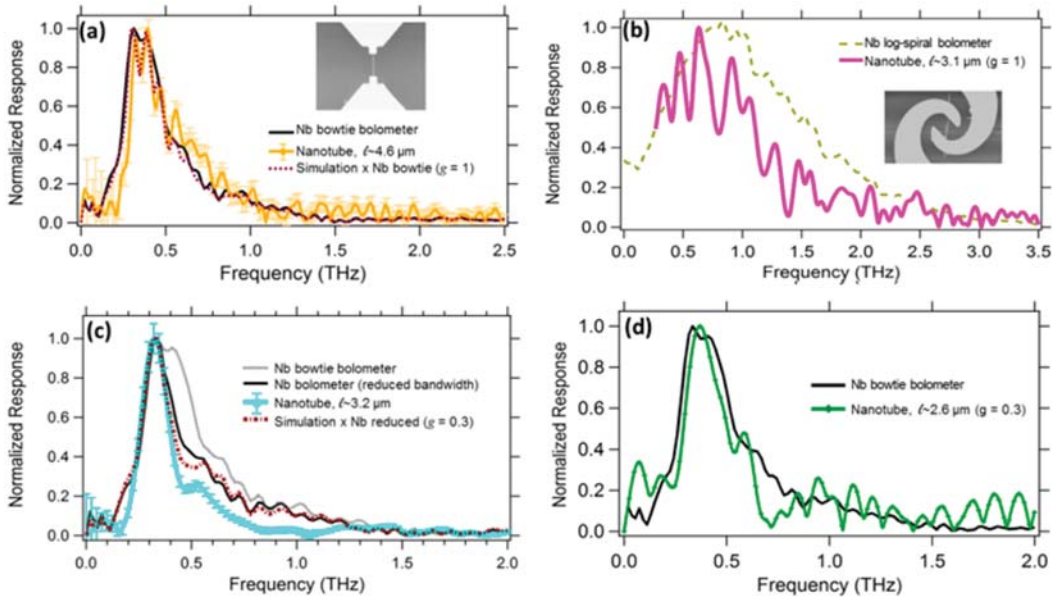

Figure 5. Normalized spectral response of (a) a 4.6 μm long nanotube device in a bowtie antenna with a bottom-gate and (b) a 3.1 μm long nanotube device in a log-spiral antenna with a bottom-gate, both exhibiting periodic features corresponding to $g \approx 1$. Results from (c) 3.2 μm long and (d) 2.6 μm long nanotube devices in a bowtie antenna with no gate electrode revealing slight features at ≈0.46 and ≈0.54 THz, both corresponding to $g \approx 0.3$, with an assumed reduced antenna bandwidth due to optical misalignment.

DOI: 10.1021/acs.nanolett.6b01485
Nano Lett. XXXX, XXX, XXX−XXX

walled carbon nanotube devices of different lengths and antenna geometries. For each sample, the bias current and gate voltage were chosen to maximize the signal-to-noise ratio. Varying these parameters did not significantly modify the features in the spectral response, although the range over which the bias current and gate voltage could be varied was limited. Only bias currents corresponding to the zero-bias anomaly (typically $\lesssim$100 nA at ~4 K) resulted in a clear THz response.[29] Most samples required a minimum gate voltage to access the metallic regime. Many of these samples exhibited gate leakage at gate voltages beyond a particular value, and the presence of gate leakage drastically degraded the signal-to-noise ratio of the rectified THz response, effectively limiting the range of possible gate voltages. The results of the devices exhibiting resonance features in their spectral response can be classified into three general categories: (1) samples exhibiting a feature in the spectral response (as observed in NT-2) corresponding to $g \approx 0.7$, (2) samples that showed a feature in the spectral response corresponding to $g \approx 1$, and (3) samples that showed a feature in the spectral response corresponding to $g \approx 0.3$. We briefly discuss representative samples for each category. Table 1 highlights the relevant properties and material parameters from the simulations for several of the devices studied.

A second sample comparable in length and resistance to NT-2, measuring ≈1.1 μm, at the center of a bowtie antenna with a side-gate shows similar behavior with a dip of ≈0.6 THz, as seen in Figure 4. This frequency also corresponds to $g \approx 0.7$. This sample has also been measured in a similar FTIR system at the University of North Florida, revealing a dip in the spectral response at the same frequency. This reproducibility in two different experimental systems demonstrates the robustness of the spectral response. A longer nanotube, 3.2 μm, with a log-spiral antenna geometry and a bottom-gate, shown in the inset of Figure 4, shows the periodicity of the dip feature in the spectral response. Measured at a bias current of I_{DC} = 5 nA and V_{gate}= −32 V, the frequency spacing of the dip features for this device is $\Delta f \approx 0.17$ THz, also corresponding to $g \approx 0.7$. Simulations of this device agree with this value of g, as shown by the dotted line in Figure 4.

A sample from the second category, for which we fit $g \approx 1$, is a 4.6 μm long nanotube device in a bowtie antenna, measured at I_{DC} = 20 nA and V_{gate} = −0.6 V, as shown in Figure 5a. Several other measurements at other bias conditions, such as 100 nA and V_{gate} = −10 V, show similar behavior but with a decreased signal-to-noise ratio. Figure 5b shows a 3.1 μm long nanotube device in a log-spiral antenna, measured at I_{DC} = 10 nA and V_{gate} = −32 V also from this category. These 4.6 and 3.1 μm long devices, as well as a 3.0 μm bowtie antenna device and a 2.3 μm log-spiral antenna device, showed frequency spacing of 0.084, 0.13, 0.13, and 0.18 THz, respectively, all corresponding to $g \approx 1$.

A pair of the samples studied show features that correspond to lower g values, e.g., the sample shown in Figure 5c,d. The sample in Figure 5c is a 3.2 μm long nanotube in a bowtie antenna with no nearby gate electrode. It was measured at I_{DC} = 100 nA and displays a slight dip within the maximum detection region at $f \approx 0.46$ THz, corresponding to $g \approx 0.3$. Similarly, the sample in Figure 5d is a 2.6 μm long device displaying a dip at $f \approx 0.54$ THz. These devices showed limited bandwidth. If this reduction in bandwidth were entirely due to a large nanotube contact capacitance, it would require a value of $C_c \approx 500$ aF, which is higher than the previous determination of the upper bound of the contact capacitance.[29] Thus, optical misalignment of the sample in the FTIR system may be a significant contributor, such that the misalignment will cause shorter wavelength radiation not to intersect the antenna. For the simulation shown in Figure 5c, we assume a reduced bolometer antenna bandwidth to match the nanotube bandwidth envelope. Nevertheless, neither a larger contact capacitance nor misalignment explains the dip feature observed in the spectral response, which is well-fit as a first resonance corresponding to $g \approx 0.3$.

Other samples displayed no noticeable resonance features within the measured frequency range (possibly due to damping from a very large internal resistance), were too noisy to reliably determine any reproducible resonant features (often the case for higher-resistance samples), did not produce a well-defined interferogram (i.e., no central peak) despite reasonable nonlinear detection, or did not show any THz response at all. These samples highlight the challenges of obtaining uniform and robust properties in individual carbon nanotube devices.

A comparison of the samples that displayed clear resonance features is shown on a single plot, Figure 6, in which the device

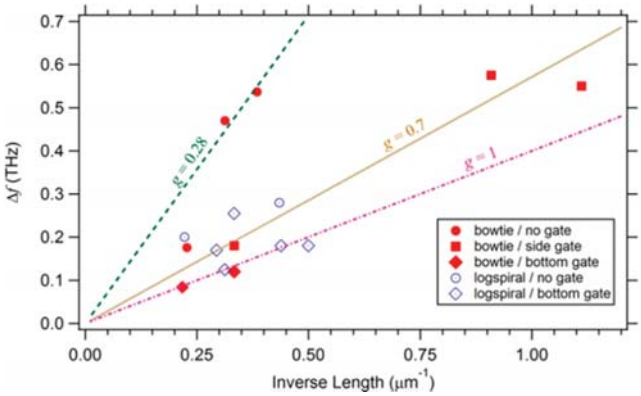

Figure 6. Plot of frequency spacing from spectral-response measurement as a function of nanotube inverse length comparing samples measured with identifiable resonance features. Several samples are best fit by a single-particle excitation given by g = 1, and two samples with no gate electrode are fit by $g \approx 0.3$; a number of devices correspond to intermediate values near $g \approx 0.7$. The antenna and gate geometries are specified in the legend.

antenna and gate geometries are also indicated. The slope of this plot of the measured resonant-frequency spacing Δf as a function of the inverse length of the device reveals the fitted value of g. A total of three distinct trends are evident. Several samples correspond to $g \approx 1$, representing the noninteracting case with propagation at v_F, consistent with the results obtained by Zhong et al.[31] A pair of samples agree with the theoretical value of $g \approx 0.3$. Half of the samples distinctly lie in between these two cases, with $g \approx 0.7$. We conclude that single-walled carbon nanotubes can indeed exhibit a charge velocity that is faster than the Fermi velocity, as predicted by Luttinger liquid theory.

Lee et al. reported on the imaging of 1D standing waves in metallic single-walled carbon nanotubes using scanning tunneling spectroscopy.[41] They describe observing electronic standing waves produced by spin-charge separation and report that $g \approx 0.55$. They explain the discrepancy between this value and the predicted theoretical value by stating that the underlying metallic substrate reduces the effective Coulomb interaction range of the electrons in the nanotube, increasing

DOI: 10.1021/acs.nanolett.6b01485
Nano Lett. XXXX, XXX, XXX−XXX

the g value accordingly. This screening by the gate electrode[42] is a possible explanation for the increased g value observed for many of our devices. As seen in Figure 6, the samples studied without a side-gate electrode show a g value closer to the predicted value of $g \approx 0.3$. All of the samples that showed $g \approx 1$ had bottom-gates. The samples with $g \approx 0.7$ primarily had side-gates or no gates. This suggests that the proximity of a relatively large metal gate electrode is a source of electron screening that can modify the electron−electron interaction strength. Testing this further would be appealing, but it is difficult because a typical experimental quasi-metallic nanotube device often requires a gate to access the fully metallic regime. The select devices studied in this work without a gate were rare samples that naturally exhibited lower resistance. Future studies of nanotubes in varying contact conditions with alternative substrates, suspended geometries, or much smaller gates may further elucidate the effect of the electromagnetic environment on the charge-propagation velocity.

Recent theoretical studies have examined the decay of a plasmon into the neutral spin modes within a carbon nanotube[43] and have taken into account other higher-order processes that go beyond the simple Luttinger liquid picture.[44,45] These processes can lead to a finite lifetime of the excitation, which would modify the total effective v_p of the overall excitation. This may generate a more-complicated picture of the expected 1D electrical behavior[46] and re-evaluation of the predicted value for g.

In summary, carbon nanotubes offer a laboratory in which to study 1D electron behavior, including the effects of strong electron−electron interactions as described by Luttinger liquid theory. One key prediction of this theory is that the fundamental low-energy excitations of the electron system are collective charge modes, or plasmons, that propagate faster than the Fermi velocity. We have studied individual micron-length antenna-coupled metallic single-walled carbon nanotubes in an FTIR spectrometer. We excite THz standing-wave resonances and measure the THz spectral response using the nonlinear nanotube contact resistance. The spectral response reveals standing-wave resonances consistent with a charge velocity v_p that is equal to the Fermi velocity for several samples and faster than the Fermi velocity for others. The v_p for some devices studied corresponds to a Luttinger interaction parameter of $g \approx 0.7$, and a few devices agreed with the theoretically predicted value of $g \approx 0.3$. We believe that the difference in the experimental values may arise from the different electromagnetic environments of the samples. A full understanding of this behavior may require that the theory be extended beyond the conventional Luttinger liquid picture. The experimental technique presented here offers a means of probing the correlated electrical properties of low-dimensional nanomaterials at THz frequencies. Understanding these properties is important for the design and realization of next-generation nanoelectronics based on 1D materials.

Methods. The fabrication of antenna-coupled single-walled metallic carbon nanotube devices for THz measurement begins with the growth of carbon nanotubes using the chemical-vapor-deposition technique on high-resistivity silicon (Si) substrates.[47] The substrates have a top silicon oxide layer and, in some cases, a bottom metal gate electrode pattern beneath the oxide, which is approximately 300 nm thick (if a side-gate will not be used). High-resistivity Si is used because the THz radiation is transmitted through the back of the substrate, and charge carriers in doped Si would drastically attenuate the THz signal. Isolated individual single-walled carbon nanotubes are located using scanning electron microscopy and atomic-force microscopy.[25] We only select nanotubes with diameters of <2 nm to avoid multiwalled nanotubes and nanotube bundles. The antenna geometry is patterned with electron-beam lithography followed by the deposition of palladium (Pd) for low contact resistance. The nanotube DC electrical properties are measured to distinguish between quasi-metallic and semiconducting nanotubes, and quasi-metallic nanotubes are selected for THz characterization. A nearby side-gate electrode can also be included for bowtie antenna samples or a bottom-gate for log-spiral antenna samples to gate quasi-metallic nanotubes into the metallic state. Remaining unwanted nanotubes, and unwanted nanotube sections for log-spiral antennas, are removed using oxygen plasma.

AUTHOR INFORMATION

Corresponding Author

*E-mail: daniel.prober@yale.edu.

Notes

The authors declare no competing financial interest.

ACKNOWLEDGMENTS

We thank P. Kim, C. McKitterick, F. Carter, M. Rooks, L. Frunzio, C. Schmuttenmaer, M. Brink, B. Connelly, M. Purewal, and M. Takekoshi for assistance and helpful discussions. We also thank P. Kim for providing the facilities for nanotube growth used for this work. The work at Yale was supported by NSF under grant no. DMR-0907082. D.S. acknowledges support from a Cottrell College Science Award from Research Corporation for Science Advancement. (J.D.C.) Present address: IBM T.J. Watson Research Center, Yorktown Heights, NY 10598, United States.

REFERENCES

(1) Bockrath, M.; McEuen, P. L.; Cobden, D. H.; Lu, J.; Rinzler, A. G.; Smalley, R. E.; Balents, L. Luttinger-liquid behaviour in carbon nanotubes. *Nature* **1999**, *397*, 598−601.

(2) Biercuk, M. J. Electrical transport in single-walled carbon nanotubes. *Topics in Applied Physics* **2007**, *111*, 455.

(3) Ilani, S.; McEuen, P. L. Electron transport in carbon nanotubes. *Annu. Rev. Condens. Matter Phys.* **2010**, *1*, 1−25.

(4) Deshpande, V. V.; et al. Electron liquids and solids in one dimension. *Nature* **2010**, *464*, 209.

(5) Tomonaga, S. Remarks on Bloch's method of sound waves applied to many-Fermion problems. *Prog. Theor. Phys.* **1950**, *5*, 544−569.

(6) Luttinger, J. M. An exactly solvable model of many-Fermion system. *J. Math. Phys.* **1963**, *4*, 1154.

(7) Tarkiainen, R.; et al. Multiwalled carbon nanotube: Luttinger versus Fermi liquid. *Phys. Rev. B: Condens. Matter Mater. Phys.* **2001**, *64*, 195412.

(8) Kane, C. L.; Fisher, M. P. A. Transport in a one-channel Luttinger liquid. *Phys. Rev. Lett.* **1992**, *68*, 1220−1223. Kane, C.; et al. Coulomb interactions and mesoscopic effects in carbon nanotubes. *Phys. Rev. Lett.* **1997**, *79*, 5086.

(9) Yao, Z.; et al. Carbon nanotube intramolecular junctions. *Nature* **1999**, *402*, 273−276.

(10) Ishii, H.; et al. Direct observation of Tomonaga-Luttinger liquid state in carbon nanotubes at low temperatures. *Nature* **2003**, *426*, 540−544.

(11) Gao, B.; et al. Evidence for Luttinger-liquid behavior in crossed metallic single-wall nanotubes. *Phys. Rev. Lett.* **2004**, *92*, 216804.

DOI: 10.1021/acs.nanolett.6b01485
Nano Lett. XXXX, XXX, XXX−XXX

(12) Tobias, D. 1/F Noise and Luttinger Liquid Phenomena in Carbon Nanotubes. Doctoral Dissertation, University of Maryland, College Park, MD, 2007.
(13) Sonin, E. B. Tunneling into 1D and quasi-1D conductors and Luttinger-liquid behavior. *J. Low Temp. Phys.* **2001**, *124*, 321−334.
(14) Jezouin, S.; et al. Tomonaga−Luttinger physics in electronic quantum circuits. *Nat. Commun.* **2013**, *4*, 1802.
(15) Matveev, K. A.; Glazman, L. I. Coulomb blockade of tunneling into a quasi-one-dimensional wire. *Phys. Rev. Lett.* **1993**, *70*, 990.
(16) Bachtold, A.; et al. Suppression of tunneling into multiwall carbon nanotubes. *Phys. Rev. Lett.* **2001**, *87*, 166801.
(17) Yi, W.; et al. Tunneling into multiwalled carbon nanotubes: Coulomb blockade and the Fano resonance. *Phys. Rev. Lett.* **2003**, *91*, 076801.
(18) Auslaender, O. M.; et al. Spin−charge separation and localization in one dimension. *Science* **2005**, *308*, 88−92.
(19) Jompol, Y.; et al. Probing spin−charge separation in a Tomonaga-Luttinger liquid. *Science* **2009**, *325*, 597−601.
(20) Plombon, J. J.; et al. High-frequency electrical properties of individual and bundled carbon nanotubes. *Appl. Phys. Lett.* **2007**, *90*, 063106.
(21) Bockrath, M.. Carbon Nanotubes: Electrons in One Dimension. Doctoral Dissertation, University of California, Berkeley, CA, 1999.
(22) Burke, P. J. Luttinger liquid theory as a model of the gigahertz electrical properties of carbon nanotubes. *IEEE Trans. Nanotechnol.* **2002**, *1*, 129−144.
(23) Pozar, D. M. *Microwave Engineering*, 3rd ed.; Wiley: New York, 2005.
(24) Yu, Z.; Burke, P. J. Microwave transport in metallic single-walled carbon nanotubes. *Nano Lett.* **2005**, *5*, 1403.
(25) Purewal, M. S.; et al. Scaling of resistance and electron mean free path of single-walled carbon nanotubes. *Phys. Rev. Lett.* **2007**, *98*, 186808.
(26) Burke, P. et al., *Selected Topics in Electronics and Systems: Nanotubes and Nanowires*; World Scientific: Singapore, 2007; DOI: 10.1142/9789812708274; Vol. *44*.
(27) Santavicca, D. F.; et al. Energy loss of the electron system in individual single-walled carbon nanotubes. *Nano Lett.* **2010**, *10*, 4538.
(28) Santavicca, D. F.; et al. Bolometric and nonbolometric radio frequency detection in a metallic single-walled carbon nanotube. *Appl. Phys. Lett.* **2011**, *98*, 223503.
(29) Chudow, J. D.; et al. Terahertz detection mechanism and contact capacitance of individual metallic single-walled carbon nanotubes. *Appl. Phys. Lett.* **2012**, *100*, 163503.
(30) Davis, S. P. et al. *Fourier Transform Spectrometry*; Academic Press: San Diego, 2001.
(31) Zhong, Z. H.; et al. Terahertz time-domain measurement of ballistic electron resonance in a single-walled carbon nanotube,. *Nat. Nanotechnol.* **2008**, *3*, 201.
(32) Ngai, D. H.; et al. *Proposal for Extracting the Luttinger Liquid Velocity in Carbon Nanotubes*; APS March Meeting 2011, abstract no. J30.015; American Physical Society: College Park, MD, 2011.
(33) Ponomarenko, V. V. Frequency dependences in transport through a Tomonaga-Luttinger liquid wire. *Phys. Rev. B: Condens. Matter Mater. Phys.* **1996**, *54*, 10328.
(34) Cuniberti, G.; et al. AC conductance of a quantum wire with electron-electron interactions. *Phys. Rev. B: Condens. Matter Mater. Phys.* **1998**, *57*, 1515.
(35) Sablikov, V. A.; Shchamkhalova, B. S. Dynamic transport of interacting electrons in a mesoscopic quantum wire. *J. Low Temp. Phys.* **2000**, *118*, 485−494.
(36) Carrion, E. et al. New Results on Terahertz Detection by Carbon Nanotubes. *Proc. 20th Int. Symp. Space Terahertz Technol.*; **2009**; pp.110−119. Carrion, E. et al. Single wall carbon nanotube (SWCNT) devices as THz detectors and mixers. *Proc. 21th Int. Symp. Space Terahertz Technol.*; **2010**; pp.312−317.
(37) Kibis, O. V.; et al. Generation of terahertz radiation by hot electrons in carbon nanotubes. *Nano Lett.* **2007**, *7*, 3414−3417.
(38) Muthee, M. Terahertz radiation from single walled carbon nanotubes. Master's Thesis, University of Massachusetts: Amherst, MA, 2011.
(39) Rutledge, D. B.; Muha, M. S. Imaging antenna arrays. *IRE Trans. Antennas Propag.* **1982**, *30*, 535−540.
(40) Santavicca, D. F.; et al. A far-infrared Fourier transform spectrometer with an antenna-coupled niobium bolometer. *Supercond. Sci. Technol.* **2007**, *20*, S398−S402.
(41) Lee, J.; et al. Real space imaging of one-dimensional standing waves: Direct evidence for a Luttinger liquid. *Phys. Rev. Lett.* **2004**, *93*, 166403.
(42) Egger, R.; Grabert, H. Electroneutrality and the Friedel Sum Rule in a Luttinger Liquid. *Phys. Rev. Lett.* **1997**, *79*, 3463.
(43) Chen, W.; et al. Decay of a plasmon into neutral modes in a carbon nanotube. *Phys. Rev. B: Condens. Matter Mater. Phys.* **2010**, *82*, 115444.
(44) Barak, G.; et al. Interacting electrons in one dimension beyond the Luttinger-liquid limit. *Nat. Phys.* **2010**, *6*, 489.
(45) Imambekov, A.; et al. One-dimensional quantum liquids: Beyond the Luttinger liquid paradigm. *Rev. Mod. Phys.* **2012**, *84*, 1253−1306.
(46) Schmidt, T. L.; et al. Spin-charge separation in one-dimensional fermion systems beyond Luttinger liquid theory. *Phys. Rev. B: Condens. Matter Mater. Phys.* **2010**, *82*, 245104.
(47) Hong, B. H.; et al. Quasi-continuous growth of ultralong carbon nanotube arrays. *J. Am. Chem. Soc.* **2005**, *127*, 15336−15337.

DOI: 10.1021/acs.nanolett.6b01485
Nano Lett. XXXX, XXX, XXX−XXX